bonds along the y axis (110), raising the energy of d_{yz} orbitals well above the level of the d_{xz} and d_{xy} orbitals. Instead of a two-thirds–filled set of threefold-degenerate t_{2g} orbitals, *lt*-$La_4Ru_2O_{10}$ contains one nearly full doubly degenerate band and one nearly empty nondegenerate band (electron configuration $d_{xy}^2 d_{xz}^2 d_{yz}^0$). This results in virtually all of the d electrons in *lt*-$La_4Ru_2O_{10}$ being paired and in the loss of the $S = 1$ magnetic moment.

The conclusion that the magnetic transition in $La_4Ru_2O_{10}$ is driven by orbital ordering is supported by other measurements. Powder neutron diffraction data rule out antiferromagnetic ordering as the cause of the magnetic transition, because of the absence of supercell reflections in the low-temperature data and because of the successful fitting of the observed data without including magnetic scattering. In some systems such as $NdNiO_3$ (*18*), sharp magnetic transitions are induced by metal-insulator transitions. However, this is certainly not the case in $La_4Ru_2O_{10}$, which is semiconducting both above and below the magnetic transition.

The formation of a spin gap in the orbitally ordered state is confirmed by inelastic neutron scattering experiments on powder samples (Fig. 4). These neutron scattering experiments are able to directly probe the nature of magnetic excitations and can readily resolve the fundamental magnetic changes upon cooling through the 160 K transition. Data on *ht*-$La_4Ru_2O_{10}$ were collected at 200 K, whereas data on *lt*-$La_4Ru_2O_{10}$ were collected at 100 K. Initial experiments using 400-meV neutrons allow the broad features of $La_4Ru_2O_{10}$ to be probed. Even on this large energy scale, it can be seen that there are substantial differences between *lt*-$La_4Ru_2O_{10}$ and *ht*-$La_4Ru_2O_{10}$. The response of *ht*-$La_4Ru_2O_{10}$ is featureless except for the broad quasi-elastic peak centered at zero energy transfer (Fig. 4A). This is not the case for *lt*-$La_4Ru_2O_{10}$, which exhibits a second peak around 40 meV, which can can be more clearly resolved when probed with 150-meV neutrons (Fig. 4B). In addition, the quasi-elastic scattering of *lt*-$La_4Ru_2O_{10}$ is greatly reduced, as can be seen in data collected at 25 meV (Fig. 4C).

The magnetic contribution to the scattering in *ht*-$La_4Ru_2O_{10}$ is best fit to a purely quasielastic peak with a width of 40.5 ± 5.4 meV. On the other hand, the fit to the scattering from *lt*-$La_4Ru_2O_{10}$ shows a significantly reduced quasi-elastic peak (with a width of 16.2 ± 2.6 meV) and a new inelastic peak centered at 41.2 ± 0.6 meV and with a width of 8.6 ± 1.6 meV. The purely quasi-elastic response of *ht*-$La_4Ru_2O_{10}$ is characteristic of gapless systems with a strongly fluctuating local moment. In contrast, the 40-meV inelastic peak is a strong indicator that a gap is present in *lt*-$La_4Ru_2O_{10}$. The reduced quasi-elastic scattering of *lt*-$La_4Ru_2O_{10}$ relative to *ht*-$La_4Ru_2O_{10}$ which results from the opening of a discrete spin gap, is seen in the 25-meV scan (Fig. 4C). It is expected that the magnetic quasi-elastic scattering in *lt*-$La_4Ru_2O_{10}$ would be further or even completely reduced at temperatures well below 100 K, where thermal excitations across the 40-meV gap are no longer contributing to the quasi-elastic peak.

The structural evidence for an orbital ordering transition in $La_4Ru_2O_{10}$ is strongly supported by magnetic susceptibility and inelastic neutron-scattering measurements. Although previous studies hinted at the importance of orbital effects, $La_4Ru_2O_{10}$ provides the first realization of a full orbital ordering transition among ruthenates. There is a strong possibility that many of the phenomena seen in orbitally ordered manganites (such as charge ordering, stripe formation, and colossal magnetoresistance) may now also be found in doped layered ruthenates. Given the large differences in magnetism between 3*d* and 4*d* transition metals, there will be important new opportunities to gain insights into the phenomena associated with orbital ordering through their comparison.

References and Notes

1. Y. Tokura, N. Nagaosa, *Science* **288**, 462 (2000).
2. H. Ichikawa, J. Akimitsu, M. Nishi, K. Kakurai, *Physica B* **281-2**, 482 (2000).
3. G. R. Blake, T. T. M. Palstra, Y. Ren, A. A. Nugroho, A. A. Menovsky, *Phys. Rev. Lett.* **87**, 245501 (2001).
4. A. E. Nikiforov, S. Y. Shashkin, M. L. Levitan, T. H. Agamalyan, *Phys. Status Solidi B* **118**, 419 (1983).
5. T. Mizokawa, D. I. Khomskii, G. A. Sawatzky, *Phys. Rev. B* **60**, 7309 (1999).
6. A. M. Goldman, *Science* **274**, 1630 (1996).
7. A. Moreo, S. Yunoki, E. Dagotto, *Science* **283**, 2034 (1999).
8. Y. D. Chuang, A. Gromko, D. Dessau, T. Kimura, Y. Tokura, *Science* **292**, 1509 (2001).
9. T. Mizokawa *et al.*, *Phys. Rev. Lett.* **87**, 077202 (2001).
10. T. Hotta, E. Dagotto, *Phys. Rev. Lett.* **88**, 017201 (2002).
11. V. I. Anisimov, I. A. Nekrasov, D. E. Kondakov, T. M. Rice, M. Sigrist, *Eur. Phys. J. B* **25**, 191 (2000).
12. O. Friedt *et al.*, *Phys. Rev. B* **58**, 847 (1998).
13. P. Khalifah, Q. Huang, H. Zandbergen, D. M. Ho, R. J. Cava, in preparation.
14. Materials and methods are available as supporting material on *Science* Online.
15. P. Khalifah *et al.*, data not shown.
16. M. Braden, G. Andre, S. Nakatsuji, Y. Maeno, *Phys. Rev. B* **58**, 847 (1998).
17. Z. Fang, K. Terakura, *Phys. Rev. B* **64**, 020509 (2001).
18. M. Imada, A. Fujimori, Y. Tokura, *Rev. Mod. Phys.* **70**, 1039 (1998).

19. Supported by NSF grants DMR-9725979 and 9974327 and by the U.S. Department of Energy, Office of Science, under contract W-31-109-ENG-38. P.K. gratefully acknowledges support from an NSF graduate fellowship. The authors thank L. Mattheiss for helpful discussions.

Supporting Online Material

www.sciencemag.org/cgi/content/full/297/5590/2237/DC1

Materials and Methods

28 June 2002; accepted 20 August 2002

Collapse of a Degenerate Fermi Gas

Giovanni Modugno,* Giacomo Roati, Francesco Riboli, Francesca Ferlaino, Robert J. Brecha, Massimo Inguscio

A degenerate gas of identical fermions is brought to collapse by the interaction with a Bose-Einstein condensate. We used an atomic mixture of fermionic potassium-40 and bosonic rubidium-87, in which the strong interspecies attraction leads to an instability above a critical number of particles. The observed phenomenon suggests a direction for manipulating fermion-fermion interactions on the route to superfluidity.

Experimental research on ultracold atoms has highlighted the marked differences of bosonic and fermionic dilute quantum gases in the basic properties (*1*). In the case of a degenerate Fermi gas, confined in a harmonic external potential, the Pauli exclusion principle forbids the multiple occupation of a single quantum state and leads to a strong effective repulsion between the identical atoms. The fermions are arranged in the trap in a cloud with relatively large spatial distribution and large kinetic energy, which can be interpreted as being the result of an outward "Fermi pressure" (*2*, *3*). This is a general property of any degenerate Fermi system; for instance, it is the mechanism that stabilizes white dwarfs and neutron stars against gravitational collapse. As a result of this pressure, a dilute atomic Fermi gas is only weakly affected by the actual interactions between particles. Conversely, a Bose-Einstein condensate (BEC) occupies only the ground state of the trap, with a narrow spatial distribution, and the presence of interactions can strongly alter its structure. Indeed, a repulsive interaction broadens the density distribution, whereas an attractive interaction can lead to a collapse for a sufficiently large number of atoms, as observed for lithium (*4*) and rubidium (*5*).

European Laboratory for Nonlinear Spectroscopy, Università di Firenze, and Istituto Nazionale per la Fisica della Materia (INFM), Via Nello Carrara 1, 50019 Sesto Fiorentino, Italy.

*To whom correspondence should be addressed. E-mail: modugno@lens.unifi.it

Another scenario has been opened by the recent production of degenerate boson-fermion mixtures (*3*, *6*–*8*). Here also the interspecies interactions can play an important role, and, in particular, the effect of the mutual interaction is predicted to be enhanced for fermions by the higher density of the bosons (*9*, *10*). Moreover, as shown by the early experiments on mixtures of superfluid ^{3}He and ^{4}He (*11*, *12*), the presence of an interaction between bosons and fermions can induce an effective attraction between fermions themselves (*13*, *14*).

Here, we show that the fermion-boson interaction can substantially affect the stability of a degenerate mixture. We performed an experiment with a mixture combining a Fermi gas of potassium atoms (^{40}K) and a BEC of rubidium atoms (^{87}Rb), in which the interspecies interaction is large and attractive (*15*). For sufficiently large numbers of atoms of both species, we observe the collapse of the Fermi gas, inferred from a sudden disappearance of K atoms.

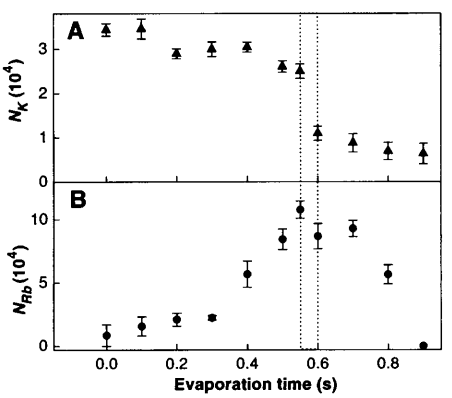

Fig. 1. Evolution of the number of potassium atoms N_K in the degenerate Fermi gas (**A**) while the number of rubidium atoms N_{Rb} in the BEC (**B**) is varied by further evaporation after the onset of condensation. At the beginning, the number of atoms in the condensate increases, and when it reaches 10^5 (highlighted region), the Fermi gas collapses and more than half of the fermions disappear from the trap. The slow decay of K before and after the collapse is due to inelastic collisions with Rb. Each data point is the average of five independent measurements. Error bars represent the standard deviation.

The mixture of degenerate gases is created by interspecies sympathetic cooling (*16*). In each experimental run, about 10^8 Rb atoms and 10^5 K atoms are laser cooled to ~100 μK in a combined magneto-optical trap, prepared in a single spin-state, and then loaded in a magnetic trap (*17*). Radio-frequency evaporation is then performed selectively on Rb, whereas K is cooled by efficient interspecies collisions. At the end of each run, the number of atoms and the momentum distribution of both samples is measured by absorption imaging after a ballistic expansion. The onset of simultaneous degeneracy of the system is reached after 25 s of evaporation, at which stage there are about 3×10^4 K atoms and 2×10^5 Rb atoms. This corresponds to a Fermi temperature (T_F) of 360 nK and to a critical temperature for condensation (T_C) of 240 nK for our trap parameters. Thermometry is performed through the measurement of the fraction of condensed atoms in the bosonic gas, and the large K-Rb thermalization rate implies thermal equilibrium between the two samples. Details of the experimental apparatus can be found in (*8*).

When the temperature is further lowered into the degenerate regime, the system is stable if the number of atoms in both species is limited to about 2×10^4, confirming the experimental findings in (*8*). When instead we increase the numbers of atoms, the picture changes markedly. In Fig. 1, we show the evolution of the number of K atoms (N_K) and of Rb atoms in the condensate fraction (N_{Rb}) during the final stage of the evaporation. The number of atoms in the condensate increases as the trap depth for Rb is lowered at a constant rate. While the condensate is still forming, we observe a relatively slow decay of K atoms on the same time scale of the evaporation, owing to inelastic collisions with Rb. However, when at time $t = 0.6$ s the condensate is completely formed, i.e., no uncondensed fraction is detectable, the number of K atoms suddenly drops to less than half its original value. The evolution of the mixture is also displayed in Fig. 2.

The features of this process give a clear indication that this is the result of a collapse of the Fermi gas. First, the duration of the drop in N_K is much shorter than the time scale of the other loss mechanisms observed in the system. For instance, the lifetime (τ) of K immediately before the drop, when $N_{Rb} \approx 7 \times 10^4$, is $\tau = 0.6(1)$ s. In contrast, when we try to span the time interval between 0.55 and 0.6 s in Fig. 1, the small shot-to-shot fluctuations of the atom numbers result in either a large ($N_K = 2 \times 10^4$) or a small ($N_K < 10^4$) Fermi gas; i.e., we are not able to observe the Fermi gas during collapse. This indicates that the collapse happens on a time $\tau \ll 50$ ms.

In addition, there is a threshold in the number of atoms in both degenerate gases for the collapse to occur. When we repeat the experiment by halving the number of K or Rb atoms (Fig. 3), we observe only a slow decay of K. For the largest Fermi gas that we can produce with a large condensate, $N_K \approx 2 \times 10^4$, the threshold for bosons is at $N_{th} \approx 10^5$ (Fig. 1). When we decrease N_K to below 1.8×10^4, we do not observe the collapse, even for the largest condensate that we can produce, with $N_{Rb} = 1.5 \times 10^5$. Additional evidence of the threshold behavior is shown in Fig. 4, where we report the evolution of N_K for an increasing number of Rb atoms in the condensate, for a series of measurements performed in the first 0.6 s of the same evaporation procedure as in Fig. 1. Here there are clearly two nonoverlapping regions for N_K, corresponding to before and after the collapse, centered around 2×10^4 and $0.5 \times$

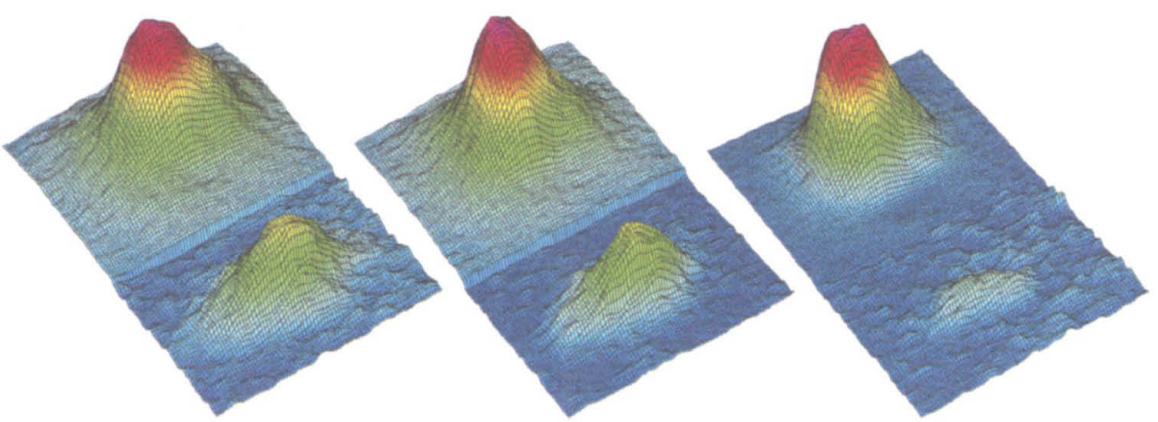

Fig. 2. False-color reconstruction of the density distributions of the Fermi (front) and Bose (back) gases during the evaporation procedure, as detected after a ballistic expansion of 4 ms for K and 19 ms for Rb. (**Left**) The BEC starts to form out of the thermal cloud and is coexisting with a relatively large Fermi gas; (**middle**) as the BEC grows larger, the Fermi gas is only moderately depleted by inelastic collisions; (**right**) when a quasi-pure condensate of 10^5 atoms has formed, the Fermi gas has already collapsed. The fermionic distributions have been vertically expanded by a factor of 3.

10^4, respectively, with a threshold for N_{Rb} at $N_{th} = 9 \times 10^4$.

To gain insight into this phenomenon, we studied the properties of samples below the collapse threshold ($N_K = 2 \times 10^4$, $N_{Rb} < N_{th}$). We found that the ballistic expansion of the two coexisting gases is different from the one measured for each of the two species alone. In particular, we observed that the aspect ratio between the radial and axial dimensions of the Fermi gas increases with the expansion time more rapidly than expected, as we previously reported also for the BEC (*8*). A numerical simulation shows that the gases behave as if they were confined in a magnetic potential with frequencies 10 to 12% larger than the actual ones.

To explain this observation, we rely on the mean-field theory of Fermi-Bose mixtures (*9*, *18*). In our experimental conditions, if K and Rb were not mutually interacting, the BEC would be completely contained in the Fermi gas, with the latter having a spatial distribution twice as large as that of the condensate (*19*). However, the boson-fermion interaction is expected to modify the topology of the system. For the K-Rb mixture we measure a large and negative interspecies scattering length (a_{BF}) of $-21.7^{+4.3}_{-4.8}$ nm (*20*), which results in a mean-field attraction between bosons and fermions, with a coupling constant (g_{BF}) = $4\pi\hbar^2 a_{BF}/2\mu$, (μ is the K-Rb reduced mass; $\hbar$ is Planck's constant divided by 2π). The corresponding interaction energy (U_F) for fermions depends on the boson density as $U_F = g_{BF}\, n_B$, whereas the reverse happens for bosons, with $U_B = g_{BF}\, n_F$. This mutual attraction is expected to lead to an increase in the density of both samples in their overlap region, as if they were more strongly confined by the magnetic trap. Although this region is small relative to the whole Fermi gas, this effect is enhanced for fermions, because the density n_B in the BEC is usually much higher than n_F (*21*). The qualitative agreement of the observation with these predictions confirms that in this mixture, the mutual attraction is sufficiently strong to counteract the Fermi pressure.

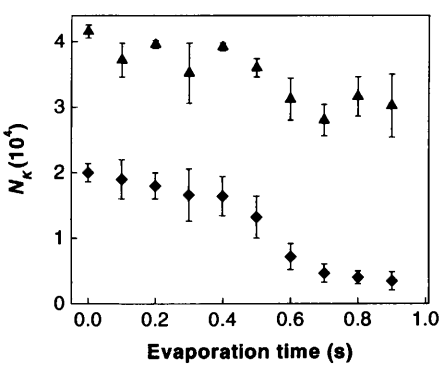

Fig. 3. Time evolution of N_K in the degenerate Fermi gas during the same evaporation procedure of Fig. 1 but starting with a smaller number of bosons (▲) or of fermions (◆). In both cases, the Fermi gas does not collapse.

In the theory, the same physical mechanism can lead to a collapse of the Fermi-Bose system: When the numbers of atoms are increased above a critical value, the repulsive energies of both gases cannot balance the attractions U_F and U_B, and the system can lower indefinitely its energy by further increasing both fermion and boson densities. For the K-Rb mixture in a simplified trap geometry and with $N_K \approx 10^4$, a collapse is predicted to occur for $N_{Rb} \approx 10^5$ for the a_{BF} given above (*22*). The qualitative agreement of the experimental observations with this model indicates that the collapse of the Fermi gas is actually driven by the boson-fermion attraction and that it is likely to be accompanied by a collapse of the BEC.

In our experiment, the Rb condensate appears to be only marginally depleted after the collapse of the Fermi gas. For example, the data in Fig. 1 show a decrease in N_{Rb} after the collapse on the order of 10^4. However, this observation can be explained by taking into account the microscopic dynamics of the collapse. As in the case of a pure BEC (*4*), the collapse of the Fermi-Bose mixture is likely to be halted at some stage by inelastic losses, which are favored by the increasing densities and rapidly reduce the atom numbers below the critical values. The comparable decrease in N_K and N_{Rb} indicates that these losses are due to interspecies collisions.

To identify the relevant collisional process involved, we studied the K losses in a nondegenerate mixture at $T = 300$ nK. We observed that K is lost only in presence of Rb, and that its loss rate scales quadratically with the Rb density n_{Rb}, whereas it is constant with N_K. This indicates that the underlying mechanism is three-body K-Rb recombination with two Rb atoms, for which we measure a rate as $K_3 = \dot{N}_K/(N_K n_{Rb}^2) = 2(1) \times 10^{-27}$ cm^6 s^{-1}.

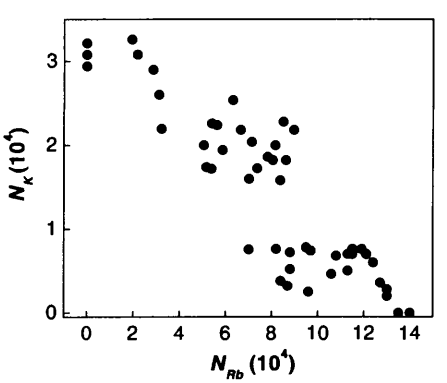

Fig. 4. Evolution of N_K in the Fermi gas as a function of N_{Rb} in the BEC, during the final stage of evaporative cooling ($t = 0$ to 0.6 s). The threshold in N_{Rb} for collapse is apparent. The gap of data in the interval $0.8 \times 10^4 < N_K < 1.5 \times 10^4$ confirms that the collapse is very rapid compared with the time scale of the evaporation.

In our system, the critical N_{Rb} for collapse can be achieved only in deeply degenerate mixtures, where no uncondensed fraction of the BEC is detectable (*23*). However, an interesting prospect would be the study of the possible role of a thermal cloud of bosons in the stability of the system.

The collapse of a Fermi gas of identical particles provides a notable signature of the major role that can be played by interactions in dilute atomic gases. Our observation indicates that the interaction between fermions can be manipulated with the use of a BEC and opens a new direction for the quest of superfluidity in fermionic gases. Indeed, the large boson-fermion attraction in K-Rb is expected to result in an effective fermion-fermion attraction (*24*). As in the case of the phonon-induced interaction between electrons in superconductors, theory predicts that this boson-induced attraction favors Cooper pairing of fermions, once prepared in a mixture of two spin states. The optimal conditions would be reached just at the onset of collapse, where the critical temperature for pairing is predicted to rise to its maximum value $T \approx 0.1 T_F$ (*24*, *25*), which could be within reach of the present experiment. This represents a promising alternative to the envisioned pairing of fermions through the direct manipulation of the fermion-fermion interaction, by means of magnetically tunable Feshbach resonances (*26*), or of strongly confining optical lattices (*27*).

References and Notes

1. See, for example, J. R. Anglin, W. Ketterle, *Nature* **416**, 212 (2002).
2. B. De Marco, D. S. Jin, *Science* **285**, 1703 (1999).
3. A. G. Truscott, K. E. Strecker, W. I. McAlexander, G. B. Partridge, R. G. Hulet, *Science* **291**, 2570 (2001).
4. C. A. Sackett, J. M. Gerton, M. Welling, R. G. Hulet, *Phys. Rev. Lett.* **82**, 876 (1999).
5. E. A. Donley *et al.*, *Nature* **412**, 295 (2001).
6. F. Schreck *et al.*, *Phys. Rev. Lett.* **87**, 080403 (2001).
7. Z. Hadzibabic *et al.*, *Phys. Rev. Lett.* **88**, 160401 (2002).
8. G. Roati, F. Riboli, G. Modugno, M. Inguscio, *Phys. Rev. Lett.*, in press; preprint available at http://arXiv.org/abs/cond-mat/0205015.
9. K. Mølmer, *Phys. Rev. Lett.* **80**, 1804 (1998).
10. M. Amoruso, A. Minguzzi, S. Stringari, M. P. Tosi, L. Vichi, *Eur. Phys. J. D* **4**, 261 (1998).
11. D. O. Edwards, D. F. Brewer, P. Seligman, M. Skertic, M. Yaqub, *Phys. Rev. Lett.* **15**, 773, (1965).
12. A. C. Anderson, D. O. Edwards, W. R. Roach, R. E. Sarwinski, J. C. Wheatley, *Phys. Rev. Lett.* **17**, 367 (1966).
13. H. Heiselberg, C. J. Pethick, H. Smith, L. Viverit, *Phys. Rev. Lett.* **85**, 2418 (2000).
14. N. J. Bijlsma, B. A. Heringa, H. T. C. Stoof, *Phys. Rev. A* **61**, 053601 (2000).
15. G. Ferrari *et al.*, *Phys. Rev. Lett.* **89**, 053202 (2002).
16. G. Modugno *et al.*, *Science* **294**, 1320 (2001).
17. K and Rb atoms are prepared in the doubly polarized states $|F = 9/2, m_F = 9/2\rangle$ and $|2, 2\rangle$, respectively. The magnetic potential has an elongated symmetry, with harmonic oscillation frequencies (ω) for Rb atoms $\omega_R = 2\pi \times 215$ Hz and $\omega_A = 2\pi \times 16.3$ Hz in the radial (*R*) and axial directions (*A*), respectively. The frequencies for K are a factor of 1.47 larger because of the smaller mass.

18. R. Roth, H. Feldmaier, *Phys. Rev. A* **65**, 021603(R) (2001).
19. For $N_{Rb} = 10^5$ and $N_K = 3 \times 10^4$, the expected dimensions of the pure BEC are $R_R = 2.8$ μm and $R_A = 37$ μm, whereas the Fermi gas is 2.2 times larger, in accordance with the experimental observation. Although the centers of mass of K and Rb are slightly displaced by gravity, their overlap is not substantially affected.
20. We measured a_{BF} by studying the damping of relative oscillations of the two species in the magnetic trap. This value is somewhat larger than the one previously measured with a different technique (*8*), though consistent also with our original prediction (*15*).
21. For $N_{Rb} = 10^5$ and $N_K = 3 \times 10^4$, the peak densities for the two noninteracting gases are $n_{Rb} = 2 \times 10^{14}$ cm^{-3} and $n_K = 8 \times 10^{12}$ cm^{-3}.
22. R. Roth, *Phys. Rev. A* **66**, 013614 (2002).
23. Given our detection limits, this corresponds to $T < 0.67T_C = 0.3T_F$.
24. L. Viverit, *Phys. Rev. A* **66**, 023605 (2002).
25. ———, S. Giorgini preprint available at http://arXiv.org/abs/cond-mat/0207260.
26. M. Holland, S. J. J. M. F. Kokkelmans, M. L. Chiofalo, R. Walser, *Phys. Rev. Lett.* **87**, 120406 (2001).
27. W. Hofstetter, J. I. Cirac, P. Zoller, E. Demler, M. D. Lukin, preprint available at http://arXiv.org/abs/cond-mat/0204237.

28. We acknowledge stimulating discussions with R. Roth, G. Shlyapnikov, and L. Viverit. Supported by Ministero dell'Instruzione, dell'Universitá e Ricerca, by the European Community under contract HPRICT1999-00111, and by INFM, Progetto di Ricerca Avanzata "Photonmatter." G.R. is also at Dipartimento di Fisica, Università di Trento; F.F. and M.I. are also at Dipartimento di Fisica, Università di Firenze; and R.B. is also at Department of Physics, University of Dayton, OH.

15 August 2002; accepted 20 August 2002
Published online 29 August 2002;
10.1126/science.1077386
Include this information when citing this paper.

Efficient Photochemical Water Splitting by a Chemically Modified n-TiO_2

Shahed U. M. Khan,* Mofareh Al-Shahry, William B. Ingler Jr.

Although n-type titanium dioxide (TiO_2) is a promising substrate for photogeneration of hydrogen from water, most attempts at doping this material so that it absorbs light in the visible region of the solar spectrum have met with limited success. We synthesized a chemically modified n-type TiO_2 by controlled combustion of Ti metal in a natural gas flame. This material, in which carbon substitutes for some of the lattice oxygen atoms, absorbs light at wavelengths below 535 nanometers and has a lower band-gap energy than rutile (2.32 versus 3.00 electron volts). At an applied potential of 0.3 volt, chemically modified n-type TiO_2 performs water splitting with a total conversion efficiency of 11% and a maximum photoconversion efficiency of 8.35% when illuminated at 40 milliwatts per square centimeter. The latter value compares favorably with a maximum photoconversion efficiency of 1% for n-type TiO_2 biased at 0.6 volt.

Since the discovery (*1*) of photoelectrochemical splitting of water on n-TiO_2 electrodes, semiconductor-based photoelectrolysis of water to hydrogen and oxygen has received much attention (*2–7*). Some applications include the use of n-TiO_2 in wet solar cells (*8–10*) and for the photodegradation of organics present in polluted water and air (*11, 12*) under ultraviolet (UV) light (wavelength $\lambda < 400$ nm) illumination, the energy of which exceeds the band-gap energy of 3.0 eV in the rutile crystalline form of n-TiO_2. Efficient photosplitting of water to hydrogen, a source of abundant clean energy, requires photoelectrodes that (i) are highly stable, (ii) are inexpensive, (iii) have a conduction band minimum that is higher than the H_2/H_2O level and a valence band maximum that is lower than the H_2O/O_2 level, and (iv) can absorb most of the photons of the solar spectrum. Although both the anatase and rutile forms of n-TiO_2 meet the first three of these conditions, they are poor absorbers of photons in the solar spectrum. Several attempts have been made to lower the band-gap energy of n-TiO_2 by transition metal doping (*13–16*) and reduction by hydrogen (*17, 18*), but no noticeable change in band-gap energy of n-TiO_2 was observed. Recently, Asahi *et al.* (*19*) reported that nitrogen doping of n-TiO_2 to n-$TiO_{2-x}N_x$ shifted its optical absorption and photodegradation of methylene blue and gaseous acetaldehyde in the visible region of $\lambda < 500$ nm.

We therefore synthesized a chemically modified (CM) n-TiO_2 by flame pyrolysis of Ti metal sheet in an attempt to lower its band-gap energy so that it could absorb the UV and most of the visible light of the solar spectrum while retaining its stability. We thermally pyrolyzed a Ti metal sheet 0.25 mm thick (Strem Co.) in the presence of combustion products [CO_2 and steam (H_2O)] in a natural gas flame with controlled amounts of oxygen added at a flow rate of ~350 ml min^{-1}. The flame temperature, measured with a digital pyrometer (Thermolyne Co.), was maintained close to 850°C by controlling the flow rates of natural gas and oxygen. The best photoresponse was obtained with a pyrolysis time of 13 min. The CM-n-TiO_2 films were dark gray, whereas the n-TiO_2 films prepared in an electric tube furnace under the same oxygen flow rate, at the same temperature and time of pyrolysis (considered here as a reference sample of n-TiO_2 film), were very light gray.

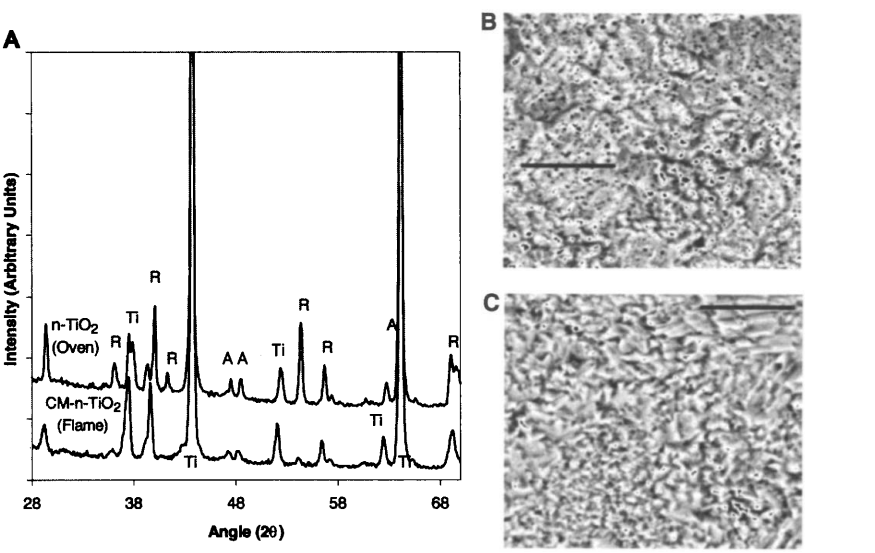

Fig. 1. (**A**) X-ray diffraction (XRD) pattern for a CM-n-TiO_2 (flame-made) and the reference n-TiO_2 (electric tube furnace– or oven-made) photoelectrodes. Ti, titanium metal; A, anatase peaks; R, rutile peaks. (**B** and **C**) SEM images of CM-n-TiO_2 (flame-made) sample (B) and reference n-TiO_2 (electric tube furnace– or oven-made) sample (C). Scale bars, 20 μm.

Department of Chemistry and Biochemistry, Duquesne University, Pittsburgh, PA 15282, USA.

*To whom correspondence should be addressed. E-mail: khan@duq.edu